*32nd URSI GASS, Montreal, 19–26 August 2017*

# Optimization-based strategy in multiple-channel magnetic resonance systems operating at 128 MHz to reduce radiofrequency heating induced by active implantable medical devices

Juan Córcoles*(1), Earl Zastrow(2), and Niels Kuster(2)(3)
(1) Universidad Autónoma de Madrid (UAM), Madrid, Spain
(2) IT'IS Foundation, Zurich, Switzerland
(3) Swiss Federal Institute of Technology of Zurich (ETHZ), Zurich, Switzerland

## Abstract

This paper presents a strategy, based on optimization techniques, to design the radiofrequency excitations in a multiple-channel magnetic resonance system operating at 128 MHz, in order to enhance radiofrequency magnetic field $|B_1^+|$ homogeneity while reducing the estimated mean induced power deposited $\langle P_{\text{ind}} \rangle$ by an active implantable medical device. Numerical examples on an implanted patient with a generic implant in different locations of a deep brain stimulator undergoing head/brain imaging are presented. Results from these examples show that more degrees of freedom (number of channels) can provide reduced induced deposited power while maintaining a high homogeneity.

## 1 Introduction

Millions of people currently live with an active implantable medical device (AIMD) inside their body. Thanks to the joint progress in engineering and medicine, medical implants have been used to enhance patients' quality of life – and in some cases sustain their lives. However, implants with elongated metallic wires (leads), such as spinal cord stimulators, deep-brain stimulators, and cardiac pacemakers, can pose a significant risk to patient if subjected to a strong radiofrequency (RF) electromagnetic field, since they are capable of picking up RF energy and depositing it in the surrounding tissues, thus resulting in unwanted heating. Therefore, Magnetic Resonance Imaging (MRI) is explicitly contraindicated for people with an AIMD. Recent efforts to assess the safety of implanted subjects undergoing this widespread medical diagnosis tool has resulted in the 2012 ISO/Technical Specification (TS) 10974:2012 [1], which is currently being revised since 2015.

Among the three magnetic fields in an MRI (static, gradient and RF), the RF magnetic field is generally circularly polarized and referred to as $B_1$, at the Larmor frequency given by the magnitude of the static magnetic field ($B_0$). The $B_1$ field has two components, $B_1^+$ and $B_1^-$ and in an efficient RF coil, $B_1^+$ significantly exceeds $B_1^-$. In order to achieve a high quality image in an MRI examination, it is desirable, among other facts, to have a homogeneous $B_1^+$ field magnitude in the Region of Interest (RoI) to be imaged. The goodness of the homogeneity of $|B_1^+|$ is measured through the homogeneity coefficient of variance (CoV), defined as the standard deviation of $|B_1^+|$ in the RoI divided over its mean value in the RoI [2].

This work presents a strategy, based on optimization techniques, to design the RF excitations in an MRI, in order to enhance $|B_1^+|$ homogeneity while reducing induced power deposited $\langle P_{\text{ind}} \rangle$ by an AIMD, estimated from a Tier 3-compliant according to ISO/TS 10974:2012 [1].

## 2 Optimization strategy

### 2.1 Best $|B_1^+|$ homogeneity

In an MRI system comprising $N_C$ channels, the total $B_1^+$ field at location $\vec{r}_i = (x_i, y_i, z_i)$ can be expressed as a weighted superposition of the fields $b_1^{(n)}$ generated by each channel $n$:

$$B_1^+(\vec{r}_i) = \sum_{n=1}^{N_C} b_1^{(n)}(\vec{r}_i) \cdot v^{(n)} = \mathbf{b}_{\mathbf{1},i}^T \mathbf{v} \qquad (1)$$

where $v^{(n)}$ is the complex excitation feeding the $n$th channel. In vector notation, $\mathbf{b}_{\mathbf{1},i}$ is a vector containing the fields from each channel while $\mathbf{v}$ is a vector containing the excitations.

By discretizing the RoI into $N_{RoI}$ points, the problem of maximizing $|B_1^+|$ homogeneity in the RoI can be stated as magnitude Least-Squares (LS) problem, which can be solved through the local-phase exchange method (LPEM) [2, 3] by casting a series of ordinary LS problems as:

$$\min_{\mathbf{v}} \quad \| |\mathbf{B_1 v}| - B \|^2 \quad \Rightarrow \quad \min_{\mathbf{v}} \quad \| \mathbf{B_1 v} - B\mathbf{t} \|^2 \qquad (2)$$

where $\mathbf{t}$ is an $N_{RoI} \times N_C$ vector whose entries have all a magnitude equal to 1 and a phase which is varied in each iteration of the LPEM to solve the magnitude LS accordingly; $\| \cdot \|$ is the $L_2$-norm of a vector, $B \in \mathbb{R}^+$ is the target mean magnitude to be achieved and:

$$\mathbf{B_1} = \left[ \mathbf{b}_{\mathbf{1},1}, \mathbf{b}_{\mathbf{1},2}, \ldots, \mathbf{b}_{\mathbf{1},i}, \ldots, \mathbf{b}_{\mathbf{1},N_{RoI}} \right]^T \qquad (3)$$

Solution to (2) provides the best homogeneity (BH) excitations $\mathbf{v}_{\text{BH}}$ which are meant to achieve the lowest CoV.

## 2.2 Maximum $|B_1^+|$ homogeneity for constrained induced deposited power $\langle P_{\text{ind}} \rangle$

In an analogous way to the magnetic field, the RF electric field tangential component to a given implant routing can be expressed as:

$$E_{\text{tan}}(\vec{r}_i) = \sum_{n=1}^{N_C} e_{\text{tan}}^{(n)}(\vec{r}_i) \cdot v^{(n)} = \mathbf{e}_{\text{tan},i}^T \mathbf{v} \tag{4}$$

The piecewise-excitation model [4, 5] estimates the induced electric $E_{\text{ind}}$ in the at-risk region of an implant through a transfer function $h(l)$ and the tangential field over its routing, which can be also discretized with $N_L$ segments to yield:

$$E_{\text{ind}} = \int_{l=0}^{L} h(l) E_{\text{tan}}(l) \mathrm{d}l \approx \mathbf{h}^T \text{diag}(\boldsymbol{\delta}) \mathbf{E}_{\mathbf{tan}} \mathbf{v} = \mathbf{g}^T \mathbf{v} \tag{5}$$

where $\mathbf{h}$ and $\boldsymbol{\delta}$ are vectors containing the transfer function value and the length of each of the $N_L$ segments, while $\mathbf{E}_{\mathbf{tan}}$ is defined as:

$$\mathbf{E}_{\mathbf{tan}} = [\mathbf{e}_{\mathbf{tan},1}, \mathbf{e}_{\mathbf{tan},2}, \ldots, \mathbf{e}_{\mathbf{tan},i}, \ldots, \mathbf{e}_{\mathbf{tan},N_L}]^T \tag{6}$$

Finally, the estimated mean induced deposited power by the AIMD including different possible $N_R$ trajectories may be computed as [6]:

$$\langle P_{\text{ind}} \rangle \approx \frac{W_0}{N_R} \|\mathbf{G}\mathbf{v}\|^2 \tag{7}$$

where each row of $\mathbf{G}$ is equal to a $\mathbf{g}^T$ in (5) computed for a different trajectory, and $W_0$ is the actual deposited power per unit tangential field, which can be derived either experimentally or numerically, by exposing the implant to an iso-electric unit tangential field.

Therefore, the problem under study can be finally formulated as [6]:

$$\begin{aligned} \text{minimize with } \mathbf{v} \quad & \|\mathbf{B_1}\mathbf{v} - B\mathbf{t}\|^2 && \text{(8a)} \\ \text{subject to} \quad & \|\mathbf{G}\mathbf{v}\|^2 \leq K \|\mathbf{G}\mathbf{v}_{\text{BH}}\|^2 && \text{(8b)} \\ & K \leq 1 \end{aligned}$$

where $K$ is a constant used to enforce an upper bound with respect to the BH case. Problem (8) can be reformulated as a real-valued second-order cone program (SOCP), which in this work is solved using the convex optimization routines from the CVXOPT Python library [7].

## 3 Numerical results

The study considers a generic 3T-MR RF high-pass birdcage transmit coil (60-cm bore, 50-cm in length, 16 legs). Virtual patient "Duke" from the the Virtual Population v3.0 [8] is situated inside it in a brain imaging position, which is set as the RoI. Two implant routings groups are considered:

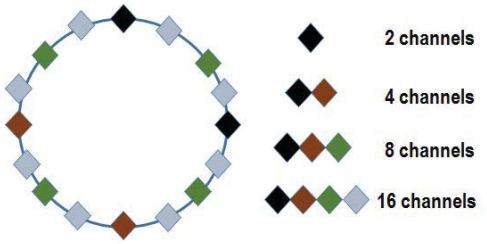


**Figure 1.** Excitation locations for the different number of channels considered in this work, all of them in the lower end-ring. For 32 channels, the upper end-ring with same locations is considered.

trajectories for a deep brain stimulator (DBS) placed on the left (DBS-L) or on the right (DBS-R), where each group has 10 different trajectories. The transfer function is that of the generic implant found in [5], which is a 400-mm long and 1.5-mm thick perfect electric conductor with a 0.5 mm-thick insulation ($\varepsilon_r$ = 3) layer, removed over a 10-mm section at one termination of the wire. For the simulations, the finite-difference time-domain software SEMCAD-X from SPEAG AG (Zurich, Switzerland) is used along with a GPU cluster.

Variability in the number of channels (2, 4, 8, 16 and 32 channels) is achieved by progressively adding more excitation locations starting from the typical IQ scheme, according to Figure 1, in the lower end-ring, up to 16 channels. For 32 channels, the upper end-ring is also excited at the same 16 locations as the lower end-ring.

To perform a fair comparison of the results provided by the different optimization strategies, all excitations are normalized to first level controlled operating mode in [9]. As a measure of the trade-off between $|B_1^+|$ homogeneity and induced deposited power $\langle P_{\text{ind}} \rangle$, we consider graphs where the $x$-axis is the CoV and the $y$-axis is the value of $\langle P_{\text{ind}} \rangle$.

Application of the LPEM to (2) in order to achieve the best $|B_1^+|$ homogeneity yields the starting points in the curves of Figures 2(a) and 2(b) for the DBS-L and DBS-R routing groups respectively. As expected, the more channels, the more homogeneous the field is. Interestingly, though no imposition or assumption has been made about this, it also looks that the best homogeneity solution with more channels provides a lower $\langle P_{\text{ind}} \rangle$, except in the transition from 8 to 16 channels in the DBS-L routing group where it increases.

Now, the SOCP (8) focused on achieving the maximum $|B_1^+|$ homogeneity while constraining the induced deposited power $\langle P_{\text{ind}} \rangle$ is applied by progressively varying the value of $K$ in (8) from 95% to 5% in steps of 10%. The results are plotted in the continuous lines in Figure 2. As expected, induced deposited power is reduced at the expense of an increased CoV in all cases. This is the same behaviour reported in [6] for a 1.5T-MR birdcage coil, operating at 64 MHz with only 2 channels (IQ), with the "Duke" model of

the Virtual Population v1.0 [10] implanted with a generic implant in the locations of a cardiac pacemaker.

It is important to note how more channels actually contribute as new degrees of freedom only if they provide an actual field diversity. For example, it is clear from Figure 1 that the new added 2 channels to the IQ excitations to conform the 4-channel setup are basically exciting the same fields (except for the inhomogeneity of the patient tissues), and thus, results in Figure 2 are almost superimposed for 2 and 4 channels.

## 4 Conclusion

An optimization strategy has been presented to reduce RF implant heating in multiple-channel MRI systems working at 128 MHz, with a tradeoff for field homogeneity in order to maintain a good image quality. Through an example, it has been shown how in overall more degrees of freedom (number of channels) can provide reduced induced deposited power while maintaining a high homogeneity.

## 5 Acknowledgements

This work was supported by the Spanish Ministry of Education under grant JC2015-00116 from the *José Castillejo* Research Mobility Programme, CICYT under contracts TEC2013-47106-C3-2-R and TEC2016-76070-C3-1-R, and UAM-Banco Santander under contract 2015/ASIA/03.

## References

[1] ISO (International Organization for Standardization), *Assessment of the safety of magnetic resonance imaging for patients with an active implantable medical device*, ISO/TS (Technical Specification) 10974:2012.

[2] I. Graesslin *et al.*, "A specific absorption rate prediction concept for parallel transmission MR" *Magn. Reson. Med.*, vol. 68, no. 5, pp. 1664–1674, Nov. 2012.

[3] K. Setsompop *et al.*, "Magnitude least squares optimization for parallel radio frequency excitation design demonstrated at 7 Tesla with eight channels," *Magn. Reson. Med.*, vol. 59, no. 4, pp. 908–915, Apr. 2008.

[4] S.-M. Park *et al.*, "Calculation of MRI-induced heating of an implanted medical lead wire with an electric field transfer function," *J. Magn. Reson. Imaging*, vol. 26, no. 5, pp. 1278–1285, Nov. 2007.

[5] E. Zastrow *et al.*, "Piece-wise excitation system for the characterization of local RF-induced heating of AIMD during MR exposure," in *Proc. Int. Symp. on Electromagnetic Compatibility, Tokyo*, 2014.

[6] J. Córcoles *et al.*, "Convex optimization of MRI exposure for mitigation of RF-heating from active medical implants," *Phys. Med. Biol.*, vol. 60, pp. 7293–7308, Sep. 2015

[7] M. S. Andersen *et al.*, "CVXOPT: a python package for convex optimization, version 1.1.6," available at `http://cvxopt.org`, 2013.

[8] M. C. Gosselin *et al.*, "Development of a new generation of high-resolution anatomical models for medical device evaluation: the Virtual Population 3.0, ," *Phys. Med. Biol.*, vol. 59, pp. 5287–5303, Sep. 2014.

[9] IEC (International Electrotechnical Comission), *Medical electrical equipment Part 2-33: Particular requirements for the basic safety and essential performance of magnetic resonance equipment for medical diagnosis* IEC Standard 60601-2-33:2010.

[10] A. Christ *et al.*, "The virtual family: development of surface-based anatomical models of two adults and two children for dosimetric simulations," *Phys. Med. Biol.*, vol. 55, no. 2, p. N23, Jan. 2010.

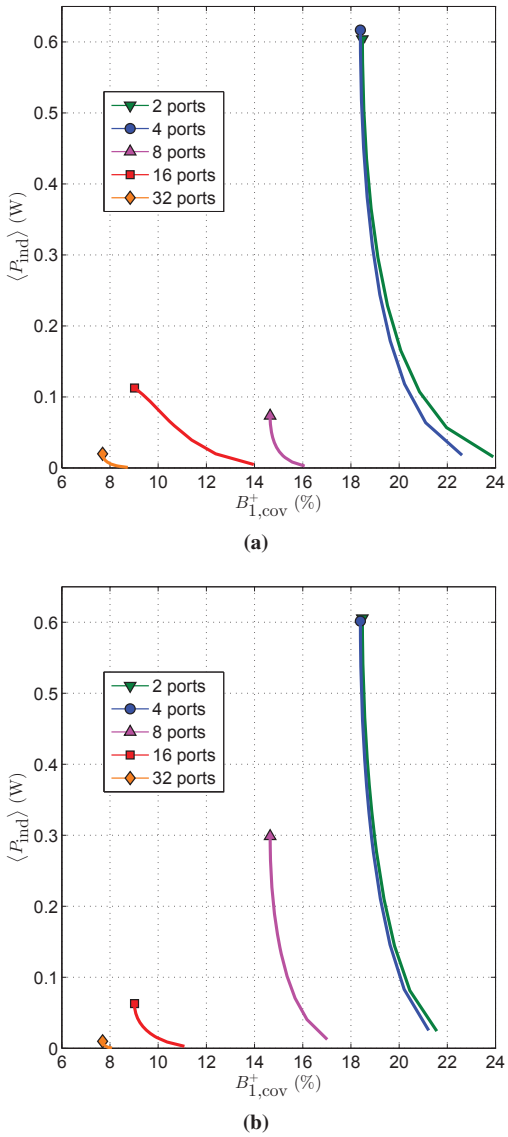


**Figure 2.** Results of the optimization-based strategy proposed in this work. Routing groups: (a) DBS-L (b) DBS-R